Adsorption and Structural Arrangement of Cetyltrimethylammonium Cations at the Silica Nanoparticle−Water Interface

Wei Wang,*,† Baohua Gu,† Liyuan Liang,†,§ and William A. Hamilton‡

Environmental Sciences and Condensed Matter Sciences Divisions, Oak Ridge National Laboratory, P.O. Box 2008, Oak Ridge, Tennessee 37831 and School of Engineering, Cardiff University, P.O. Box 925, Cardiff, CF24 0YF, United Kingdom

Received: April 16, 2004; In Final Form: August 23, 2004

Although the sorption of cetyltrimethylammonium ion (CTA^+) on silica (SiO_2) surfaces has been studied extensively, little is known about the interactions between large surfactant molecules and nanosized colloidal particles with a high specific surface area. The aim of the study was to understand the effects of structural arrangements of sorbed CTA^+ ions on the stability and surface properties of SiO_2 nanoparticles. The extent of the effect of CTA^+ sorption on the aggregation behavior of the SiO_2 nanoparticle suspension was investigated with the dynamic light scattering (DLS) technique. Both the Fourier transform infrared (FTIR) and Raman spectroscopic techniques were used to probe the sorbed layers of CTA^+ on silica surfaces. Results indicate that, at a low surface coverage (less than a monolayer), CTA^+ molecules were strongly bound to the SiO_2 surface via their trimethylammonium headgroups. A bilayer sorption of CTA^+ was observed at a high surface coverage, and the sorption is attributed to the hydrophobic interactions between aliphatic tails of CTA^+. Sorption of CTA^+ at a low surface coverage also caused the destabilization of the SiO_2 nanoparticle dispersion as a result of surface charge neutralization, but redispersion and surface charge reversal of SiO_2 colloids occurred at a high surface coverage. The present study thus confirms the adsorption mechanism of the reverse orientation model and contributes to a better understanding of the sorption and structural arrangements of sorbed surfactants at the SiO_2 nanoparticle−water interface.

Introduction

Adsorption of surfactants onto solid−liquid interfaces concerns many applications including detergency, wetting, selective flotation of minerals, lubrication, stabilization of solid dispersions, and protection of metal surfaces.[1,2] In the past several decades, adsorption of ionic surfactants at the silica−water interface has been extensively studied.[3−24] The surfactant adsorption density, the resultant zeta potential, and the observed dispersion stability have been used to infer the adsorption mechanisms.[3−10] Additionally, spectroscopic and microscopic methods, such as infrared spectroscopy,[11−13] electron spin resonance,[14−16] fluorescence spectroscopy,[3, 17] atomic force microscopy,[18−20] and neutron scattering and reflectometry,[21−24] have been applied to aid in understanding of the structural arrangement of the adsorbed surfactants at the interface. Several models describing the behavior of ionic surfactants at metal oxide surfaces have been proposed, such as the reverse orientation model suggested by Somasundaran et al.,[16,25] the surface bilayer model presented by Harwell et al.,[26] and the small surface micelle model proposed by Gu et al.[27,28] These models often assume electrostatic interactions with the formation of surface hemimicelles, local bilayer or small micelles at low surfactant solution concentrations, and a dense bilayer or micelle structure at higher concentrations.

Most of the previous studies of surfactant adsorption on silica have used large quartz or micron-sized SiO_2 particles, that is, particles with a limited specific surface area. Although some studies have explored with nanosized SiO_2 particles,[3−5,8,11,14,15,21,22] the polydispersed colloids could not give quantitative information on colloidal size evolution induced by surfactant adsorption. Information on the interactions between large surfactant molecules and nanosized colloidal particles with a high specific surface area is still greatly lacking. The highly curved surface exposed to surfactant sorption and the presence of a large fraction of uncoordinated Si and O atoms on the surface of silica nanoparticles could change the sorption behavior and spatial assemblies of surfactants and therefore the stability of nanoparticle colloidal dispersions. An understanding of sorption and structural conformation of the surfactants on the surfaces of nanoparticles is thus needed for a predictive description of nanoparticle colloid stability, which has wide application in the areas of nanoscale materials and environmental processes.

The present study therefore was aimed at a better understanding of the interactions and conformational arrangements of cationic surfactant at the SiO_2 nanoparticle−water interface, using cetyltrimethylammonium bromide (CTAB) as a model surfactant. We synthesized highly monodispersed SiO_2 nanoparticles, which allow quantitative monitoring of the effects of surfactant sorption on particle size and coagulation. Fourier transform infrared (FTIR) and Raman spectroscopic techniques were used to provide direct spectroscopic evidence of the structural arrangements of sorbed cations, either in monolayer or bilayer configurations. The extent of surfactant sorption on the aggregation behavior of the nanoparticle suspension was investigated with the dynamic light scattering (DLS) technique.

* To whom correspondence should be addressed. E-mail: wangw@ornl.gov.
† Environmental Sciences.
‡ Condensed Matter Sciences.
§ Cardiff University.

10.1021/jp048325f CCC: $27.50
Published on Web 10/15/2004

Experimental Section

Materials. Tetraethyl orthosilicate (TEOS, ≥99%) and CTAB (≥99%) were purchased from Fluka. Absolute ethanol (AR) was obtained from EM Scientific, and $NH_3 \cdot H_2O$ (29.5%) was purchased from J. T. Baker. All chemicals were used as received. Deionized water with 18.2 MΩ·cm resistivity was processed from a Millipore ultrapure water system.

Colloid Synthesis. Monodispersed colloidal SiO_2 spheres were prepared by hydrolysis of TEOS in an alcohol medium in the presence of water and ammonia, according to a procedure originally described by Stöber et al.[29] Hydrolysis and condensation of the TEOS monomers catalyzed by ammonia provide stable spherical SiO_2 nanoparticles. In the preparation, two solutions of equal volume were rapidly mixed under vigorous stirring. One of the solutions contained ethanol and TEOS and the other included ethanol, water, and ammonia. The total volume of the solutions was 250 mL with final concentrations of 9.0 M H_2O, 0.12 M NH_3, and 0.2 M TEOS. The reaction was allowed to continue for 6 h with moderate stirring at room temperature for completion, followed by heating of the samples at 98 °C for 2 h.

After the synthetic reaction was completed, the SiO_2 particles were collected and purified to eliminate ionic species and solvents by repeatedly washing with deionized water. In these cleaning cycles, a centrifuge was used for the solid−liquid separation, and a vortex mixer and an ultrasonication bath were used to redisperse the particles. The washed SiO_2 colloids were further purified in deionized water using dialysis tubes (Pierce Snake Skin, 10 000 molecular weight cutoff) to remove residual nonaqueous solvent molecules and ionic impurities. The deionized water was changed daily until its conductivity became constant (after approximately 2 weeks). The purified SiO_2 colloid dispersion was then used for surfactant sorption experiments.

Measurement. Direct imaging of SiO_2 nanoparticles was obtained by a Hitachi F 4000 transmission electron microscope (TEM) under an acceleration voltage of 200 kV. A drop of colloidal suspension was placed on a Formvar/carbon film supported by a 300-mesh copper grid (Ted Pella, Ltd.), and the solvent was allowed to evaporate to obtain a dry sample.

The average particle size, size distribution, and zeta (ζ) potential of SiO_2 colloids were determined by DLS using a Brookhaven 90Plus/ZetaPlus instrument.

The BET surface area of the SiO_2 nanoparticles was determined by nitrogen adsorption experiments on dry samples with a Micromeritics Gemini 2375 automatic gas adsorption instrument.

The molecular headgroup area of CTAB was determined using the Langmuir−Blodgett method with a Labcon Mini Langmuir trough. The CTAB chloroform solution was spread at the air/water interface. After the solvent evaporated, the surface pressure−molecular area ($\pi - A$) isotherm was measured at 23 °C with a compression rate of 200 $cm^2\ min^{-1}$.

The adsorption of surfactant molecules on SiO_2 surfaces was determined by the difference between the amounts of surfactant added and the amounts remaining in the solution phase after sorption. Purified SiO_2 colloids (1.0 wt %) were first mixed with the aqueous surfactant solution. The mixture was shaken for 30 min and allowed to stand for at least 6 h for the sorption to complete. The surfactant sorbed colloidal particles were then separated by centrifuge, and the supernatant was collected for the total organic carbon (TOC) analysis using a Shimadzu 5000A TOC analyzer. The measured TOC concentrations were converted to molar concentrations of CTAB per gram SO_2 which were used to calculate the amount of surfactant adsorbed at equilibrium.

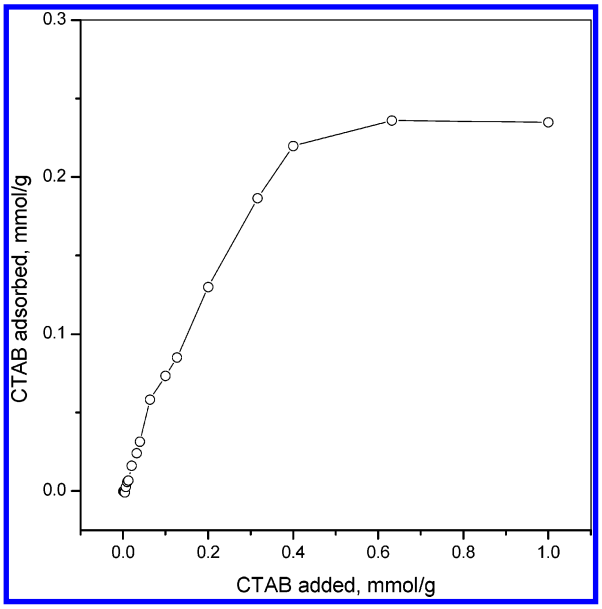

Figure 1. Adsorption of CTA^+ cations on SiO_2 nanoparticles (d = 106 nm) in deionized water at 23 °C.

For IR spectral analysis, a wet SiO_2 colloid sample collected from the colloidal suspension by centrifuge was smeared on the ZnSe crystal substrate and dried to form a colloidal-particle cast film. The IR spectra of surfactant adsorbed SiO_2 particles were recorded at 4 cm^{-1} resolution with a Nicolet Magna-760 FTIR spectrometer with a liquid nitrogen cooled MCT detector. The spectra were normalized with the intensity measured at 1104 cm^{-1}, which is stable and the strongest band from SiO_2 nanoparticles.

To obtain Raman spectra, wet SiO_2 colloid samples were first separated from colloid suspension by centrifugation and then placed between two quartz cover slides. Raman spectra were taken at 2−4 cm^{-1} resolution using a Renishaw Raman Imaging Microscope with a 785-nm NIR diode laser and a charge-coupled-device (CCD) array detector. A laser beam was focused on the sample with an area of ∼1−2 μm^2.

Results and Discussion

Extent of CTAB Adsorption on SiO_2 Nanoparticles. Sorption of CTAB on silica nanoparticles was studied in water at circumneutral pH conditions (Figure 1). As can be expected, CTA^+ was strongly sorbed as a result of electrostatic interactions between negatively charged SiO_2 particles and positively charged CTA^+ ions. The sorption reached its maximum capacity or plateau at ∼0.24 mmol g^{-1} of adsorbed CTAB, corresponding to an adsorption density of ∼1.87 mg m^{-2}. This sorption density is comparable to data reported in the literature, which typically range from 1.5 to 2.2 mg m^{-2} for adsorbed CTAB on SiO_2.[9,30,31] Using the measured specific surface area of SiO_2 nanoparticles (i.e., 46.9 $m^2\ g^{-1}$ by the BET-N_2 sorption technique), an equivalent surface area occupation was calculated to be ∼0.32 nm^2 per CTA^+ molecule by assuming a monolayer surface coverage. However, the measured molecular cross section area of CTAB headgroups at the water/air interface is ∼0.59 nm^2 using the Langmuir−Blodgett technique. This is nearly twice the calculated surface area occupation per CTA^+ molecule,

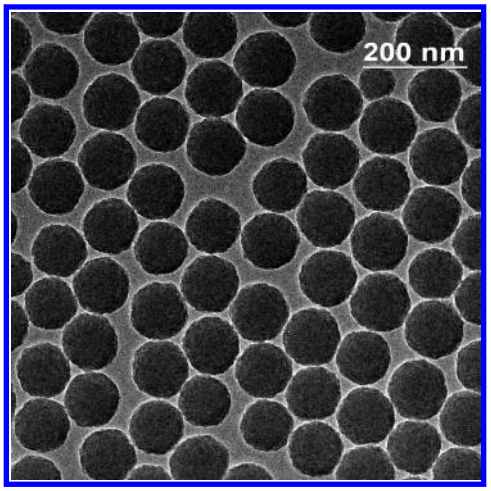

Figure 2. TEM images of synthesized SiO_2 nanoparticles. Particle size: 106 ± 5.6 nm.

suggesting that a bilayer of CTA^+ molecules may have formed at the silica nanoparticle−water interface at maximum adsorption.

Because the synthesized nanoparticles are highly uniform with an average diameter of 106 ± 5.6 nm, as shown by TEM image in Figure 2, the geometric surface area of these particles can also be calculated: ∼26.2 $m^2\ g^{-1}$. Assuming a particle density of 2.16 g cm^{-3} for amorphous Stöber silica,[32] the calculated area is approximately 44% less than that measured by the BET N_2-adsorption technique. If this geometric surface area were used to calculate CTAB adsorption, more than a bilayer of CTA^+ molecules would have accumulated at the SiO_2 surface. The discrepancy between the BET-measured specific surface area and that deduced by geometric calculation suggests that the synthesized silica nanoparticles were porous. The Stöber method produces amorphous SiO_2 colloids with both micropores and mesopores ranging from a few angstroms up to tens of nanometers.[32,33] The heating process in our synthesis could collapse micropores but still retain mesopores. It is therefore not surprising that the measured BET surface area was nearly twice that calculated by assuming silica nanoparticles as nonporous solid spheres. As a result, a large percentage of CTA^+ molecules could have been sorbed within those mesopores of silica nanoparticles. Therefore, we used the BET areas as effective surface area in our discussion.

Effects of CTAB Sorption on Surface Charge and Colloid Stability of SiO_2 Nanoparticles. Without CTAB addition, silica particles were well dispersed in water with an average particle diameter of ∼120 nm and a 3.2% polydispersity. The DLS measurements give a somewhat larger hydrodynamic particle size (∼120 nm) than that determined by TEM (∼106 nm) because of loss of the hydration layer when samples were dried for TEM measurements. Sorption of CTA^+ molecules resulted in the destabilization of the silica colloidal dispersion and the surface charge reversal (Figure 3). At added CTAB concentrations below ∼0.1 mmol g^{-1}, the nominal colloid particle size measured by DLS gradually increased with an increase in CTAB concentration. Between 0.1 and ∼0.2 mmol g^{-1}, a dramatic increase in the particle size and polydispersity was observed. A further increase in CTAB concentrations from ∼0.2 mmol g^{-1} resulted in a decrease in the overall particle size to ∼260 nm with ∼20% polydispersity. DLS analysis shows that colloidal particles with an average size of 260 nm consist of a majority of particles (∼90%) 120−140 nm in size and a few aggregated large particles >500 nm in size.

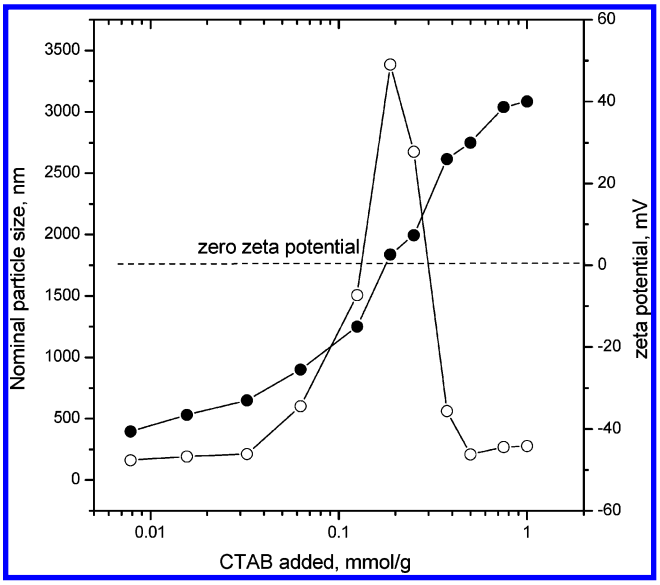

Figure 3. Effects of CTAB sorption on nominal colloidal particle sizes (open circle) and corresponding ζ potentials (solid circle) as determined by dynamic light scattering measurements. Silica colloid concentration is 0.5 wt %.

The measured ζ potential of SiO_2 colloids in the absence of CTAB was around −50 mV because the reported zero point of charge (ZPC) for SiO_2 colloids is at pH ∼ 2, above which the SiO_2 colloids are negatively charged.[34] The magnitude of ζ potential therefore decreased rapidly with an increase of CTAB sorption. A zero ζ potential was obtained at a concentration of ∼0.18 mmol g^{-1} of added CTAB, implying the surface charge was completely screened with CTAB adsorption (Figure 3). At this CTAB concentration, the sedimentation rate of the colloid reached a maximum, indicating a complete coagulation of silica nanoparticles. TOC measurement showed that the adsorbed amount of CTA^+ at the maximum sedimentation rate is ∼0.12 mmol g^{-1}. This adsorption amount roughly corresponds to CTA^+ monolayer formation on SiO_2 nanoparticles with 92.5% surface coverage. A further increase of CTAB concentration resulted in surface charge reversal. At a concentration of 1 mmol g^{-1} of added CTAB, the ζ potential of particles reached +40 mV, and a nearly complete redispersion of the silica colloids was observed.

These results are consistent with previous studies showing the dispersion−flocculation−redispersion sequence of SiO_2 colloids with the addition of cationic surfactants[1,6] and of the positively charged particles with the addition of anionic surfactants, such as sodium dodecyl sulfate (SDS)/alumina system.[1] At a low surfactant concentration, the favorable electrostatic attraction between the adsorbates and the charged surface is the main driving force. However, in concentrated surfactant solutions, how the charged surface facilitates the surfactants' interactions with themselves and what kind of association these surfactants form in the solid−water interface are yet to be determined and validated. Several models have been proposed to characterize the spatial association of surfactant molecules at charged surfaces, including the reverse orientation, bilayer, and small micelle models.

According to the reverse orientation model,[16,25] surfactants first adsorb electrostatically as individual ions, then associate into hemimicelles. In the hemimicelles, the surfactants attached their headgroups to the charged surface and oriented their tail groups toward solution, thus forming hydrophobic patches on the surface. Further adsorption then brings an increasing number of surfactants to the interface to form a second layer of bilayer

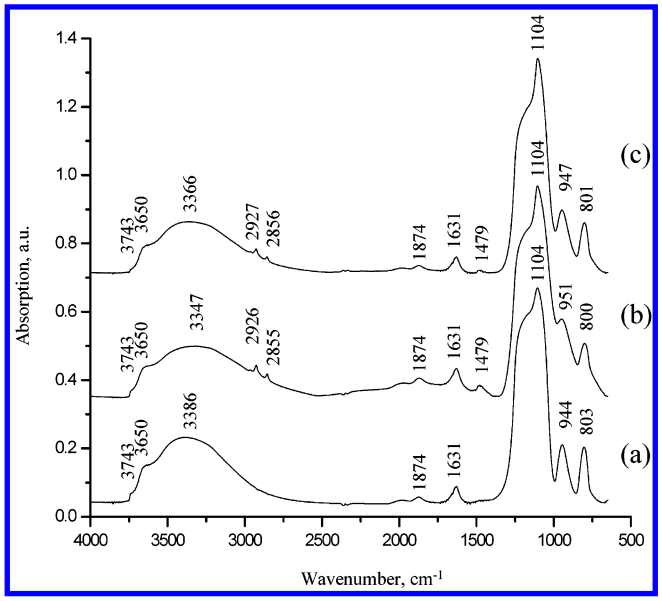

Figure 4. FTIR spectra of (a) pure SiO_2 nanoparticles, (b) SiO_2 nanoparticles sorbed with CTA^+ molecules (~0.24 mmol g^{-1}), and (c) the same sample as b, but after water washing.

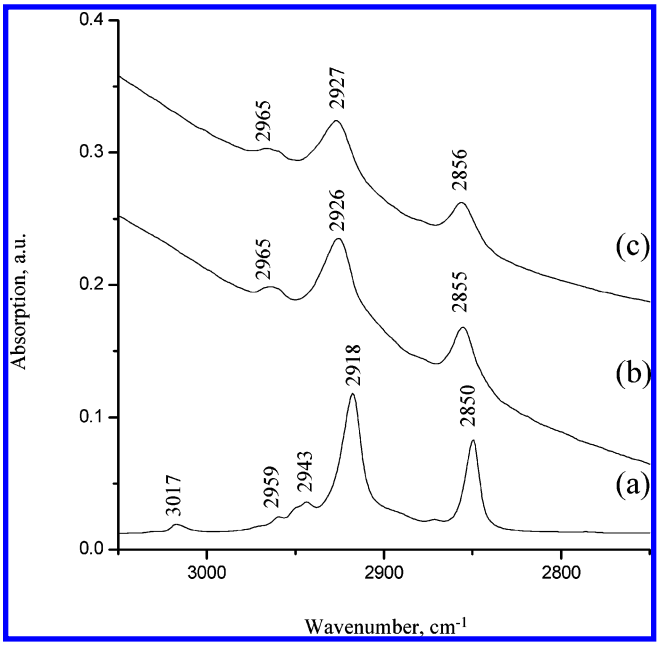

Figure 5. Expanded FTIR spectra of (a) reagent crystalline CTAB, (b) CTA^+ sorbed onto SiO_2 nanoparticles (at ~0.24 mmol g^{-1}), and (c) the same sample as b, but after water washing.

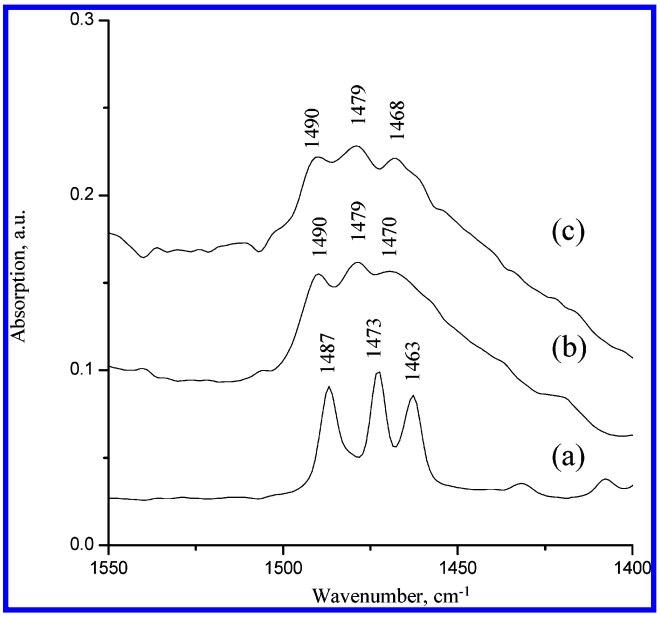

Figure 6. Expanded FTIR spectra of (a) reagent crystalline CTAB, (b) CTA^+ sorbed onto SiO_2 nanoparticles (at ~0.24 mmol g^{-1}), and (c) the same sample as b, but after water washing.

on silica surfaces. These surfactants interact through their tail groups with the existing adsorbed surfactants, reversing their orientation with headgroups facing the solution. The bilayer model[26] assumes that local bilayer structures form patches on the solid surfaces at a critical solution concentration without the formation of hemimicelles. These patches of surfactant bilayers were called admicelles. With increased surfactant adsorption, both the number and the size of the admicelles increase and they eventually form a more or less complete bilayer. Finally, in the small micelle model,[27] the initially adsorbed surfactant molecules are proposed to increase the adsorption of surfactants to form small "surface micelles" on solid surfaces. The small micelles retain their structure but become more closely packed with further adsorption. These models have been successful in describing adsorption isotherms, although the modes of adsorption may be categorized as "complete" or "patchy" bilayers at maximum adsorption.

Spectroscopic Characterization of Adsorbed CTA^+ on SiO_2 Nanoparticles. To validate the model, the structural arrangement and conformation of adsorbed CTA^+ on the SiO_2 nanoparticles were then examined by FTIR and Raman spectroscopic analyses (Figures 4−8). For pure SiO_2 nanoparticles (Figure 4a), the FTIR spectrum in the 3800−2500 cm^{-1} range is characterized by a broad peak centered at 3386 cm^{-1} and can be assigned to the O−H stretching vibration of H-bond surface hydroxyls and water.[35,36] Two shoulder bands at 3650 and 3743 cm^{-1} may be assigned to the O−H stretching mode of the isolated surface silanol groups. The complex structured absorption bands in the 3750−3000 cm^{-1} are typical for natural fine quartz powders.[35] In the 2000−800 cm^{-1} region, there are a series of absorption bands related to Si−O vibrations. The strongest band at 1104 cm^{-1} with a shoulder around 1230 cm^{-1} is due to the asymmetric Si−O stretching mode of the body Si−O−Si bridge band. This band was therefore used as an internal reference for the normalization of all spectra in Figure 4 for comparison. The bands with medium intensities at 944 cm^{-1} and 803 cm^{-1} are associated with stretching vibrations of surface Si−O bonds.

For silica nanoparticles sorbed with CTA^+ molecules (Figure 4b and c), the following characteristic absorption bands were observed: the C−H stretching modes in 3000−2800 cm^{-1}, the CH_2 bending mode, and the $CH_3-(N^+)$ deformation modes 1500−1450 cm^{-1}.[37,38] In addition, in the presence of CTA^+, the O−H stretching vibration band at 3386 cm^{-1} significantly shifted to a low frequency and broadened, and surface Si−O vibration bands at 944 cm^{-1} and 803 cm^{-1} also shifted by several wavenumbers, indicating strong interactions between CTA^+ and SiO_2 surfaces. The spectral information gives unambiguous evidence of adsorbed CTA^+ on the SiO_2 nanoparticles, even after the colloid is washed by water.

Additional insights regarding sorbed CTAB molecular conformation on silica surfaces are provided by a close examination of the spectral details in regions of 3050−2750 cm^{-1} and 1550−1400 cm^{-1} (Figures 5 and 6). The spectrum of pure solid CTAB is also given as a reference (Figures 5a and 6a). The asymmetric and symmetric stretching modes of the headgroup $CH_3-(N^+)$

are at 3017 and 2943 cm^{-1}, respectively, while the band at 2959 cm^{-1} is the asymmetric stretching mode of the CTAB terminal CH_3 group for solid CTAB (Figure 5a).[38] However, for sorbed CTA^+ on SiO_2 colloids, the 3017 cm^{-1} band disappeared, and the 2959 cm^{-1} and 2943 cm^{-1} bands merged to a new band at 2965 cm^{-1}. In the 1550−1400 cm^{-1} region of the same spectrum, the $CH_3-(N^+)$ asymmetric deformation modes of CTA^+ at 1487 and 1473 cm^{-1} blue-shifted to 1490 and 1479 cm^{-1}. These spectral changes of the headgroup $-N^+(CH_3)_3$ clearly demonstrate its strong interactions with SiO_2 surfaces and suggest that CTA^+ ions were sorbed via their headgroups. These structural characteristics of the adsorbed CTA^+ on SiO_2 colloid are also similar to those of CTA^+ in an aqueous liquid crystal state.[37]

The amount of CTA^+ sorbed on the SiO_2 surface is proportional to the normalized spectral intensity. Comparing the spectra of CTA^+ adsorbed on SiO_2 before and after water washing, the CTA^+-related spectral intensities were reduced after washing, but the basic spectral characteristics still remained. This indicates a strong interaction between the first layer of the CTA^+ and SiO_2 surface, but the upper layers were broken by water washing. The spectral evidence also supports the hypothesis that the adsorbed layer of CTA^+ is at least more than a monolayer. When the samples were repeatedly washed by water with sonication, CTAB signals completely disappeared in the IR spectrum, which suggests that there is no specific chemical bonding between the CTA^+ and SiO_2, except the electrostatic interaction.

The CH_2 stretching modes are very sensitive to hydrocarbon chain conformational ordering and mobility.[39,40] The high frequencies of the bands indicate an increase of conformational disorder, depending on the content of gauche conformers in the average orientation, while the bandwidth is proportional to the degree of the molecular mobility within the layer. For solid CTAB, the CH_2 asymmetric and symmetric stretching modes appear at 2918 cm^{-1} and 2850 cm^{-1}, respectively. In comparison with the pure CTAB, the two bands widened and shifted to high frequencies at 2926 cm^{-1} and 2855 cm^{-1} for sorbed CTA^+ on SiO_2 colloids. This implies that the packing of CTA^+ on the SiO_2 particle surface was not rigid, as in the solid state, and the hydrocarbon chains were mobile within the molecular layers. For washed samples, the two bands further blue-shifted ~1 cm^{-1}, implying a weakened hydrophobic interaction between hydrocarbon chains. This result suggests that the interaction between the first and second adsorbed layers was attributable to hydrophobic forces between the CTA^+ tail groups.

The CH_2 scissoring band is sensitive to intermolecular interaction and therefore is often used to indicate the state of packing of the hydrocarbon chain.[41,42] For crystal CTAB, the CH_2 scissoring mode is split into a doublet at 1473 and 1463 cm^{-1} because of intermolecular interaction between two adjacent hydrocarbon chains in an orthorhombic perpendicular subcell, although the 1473 cm^{-1} component may overlap with the $CH_3-(N^+)$ deformation mode at the same frequency (Figure 6). For sorbed CTA^+ on SiO_2 particles, the spectrum showed a single band at 1470 cm^{-1}, which is indicative of a dense subcell packing where the hydrocarbon chains were packed in a parallel arrangement and had a strong chain interaction. The strong chain interaction suggests the bilayer structure in which the first and second layers attached to each other by the aliphatic tails of CTA^+ molecules. After the colloid was washed, the single band shifted to 1468 cm^{-1}, which is characteristic of a relatively disordered hexagonal subcell packing where the hydrocarbon chain freely rotates around its long axis. This observation

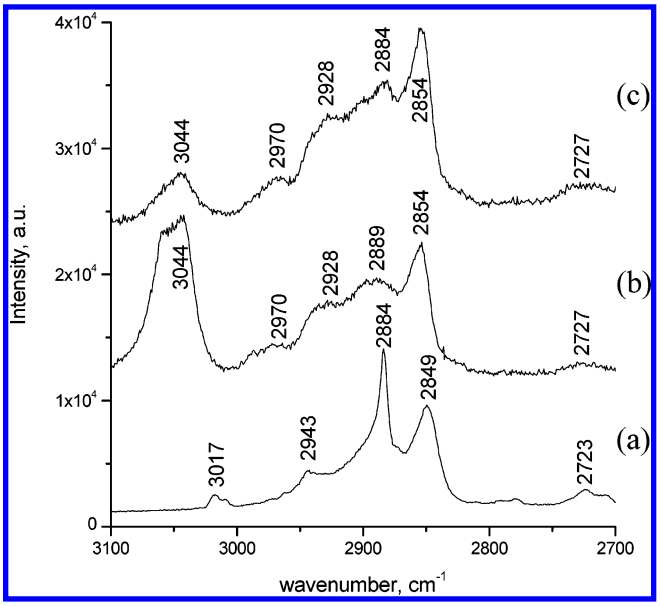

Figure 7. Raman spectra of (a) reagent crystalline CTAB, (b) wet silica nanoparticles with sorbed CTA^+ at approximately a monolayer surface coverage, and (c) wet silica nanoparticles with sorbed CTA^+ at approximately a bilayer surface coverage.

suggests that the bilayer had been disrupted, and only a monolayer of CTAB remained on SiO_2 surfaces.

Raman spectroscopy was also employed as a complementary technique to FTIR spectroscopy because FTIR spectra obtained from the dry colloids may not be fully representative of surfactant structures and orientations on SiO_2 surfaces. Raman spectroscopy has advantages that allow measurement of the spectra of adsorbed CTAB on SiO_2 in the presence of water. The wet state is much closer to the real adsorption environment, and no scattering signals came from free surfactant molecules in the equilibrium solution. Wet colloidal samples separated by centrifugation were used for the Raman spectroscopic measurement. Figures 7 and 8 show the spectra of silica nanoparticles sorbed with an approximate bilayer of CTAB (at 0.24 mmol g^{-1} sorbed CTAB) and an approximate monolayer of CTAB (at 0.12 mmol g^{-1} sorbed CTAB), along with spectra of pure CTAB and pure wet SiO_2 colloids for comparison. In the high-energy region (Figure 7), the $CH_3-(N^+)$ asymmetric stretching mode of pure CTAB solids occurred at 3017 cm^{-1}, but it dramatically shifted to 3044 cm^{-1} for sorbed CTA^+ on SiO_2. Additionally, the relative intensity of this band was the strongest for sorbed CTA^+ at the monolayer surface coverage, suggesting strong interactions between SiO_2 and CTA^+ headgroups. For sorbed CTA^+ at the bilayer surface coverage, however, the band intensity was lower. These results are consistent with the FTIR measurements and support the hypothesis of a bilayer formation (at its maximum sorption capacity).

The spectral features at around 2885 and 2850 cm^{-1} were attributed to the symmetric and asymmetric CH_2 stretching modes of CTAB molecules. The peak intensity ratio at I_{2885}/I_{2850} has generally been used to measure the lateral order of hydrocarbon chains and provides information on chain packing and chain mobility.[43,44] For pure solid CTAB (Figure 7a), the symmetric mode at 2884 cm^{-1} is more intense than the asymmetric mode at 2849 cm^{-1}, and the intensity ratio is about 1.5. However, this order was reversed for CTA^+ sorbed on silica surfaces (Figure 7b and c), and the intensity ratio decreased to ~0.7, suggesting a relatively high mobility of the hydrophobic tail groups in CTA^+ molecules on the SiO_2 surface.

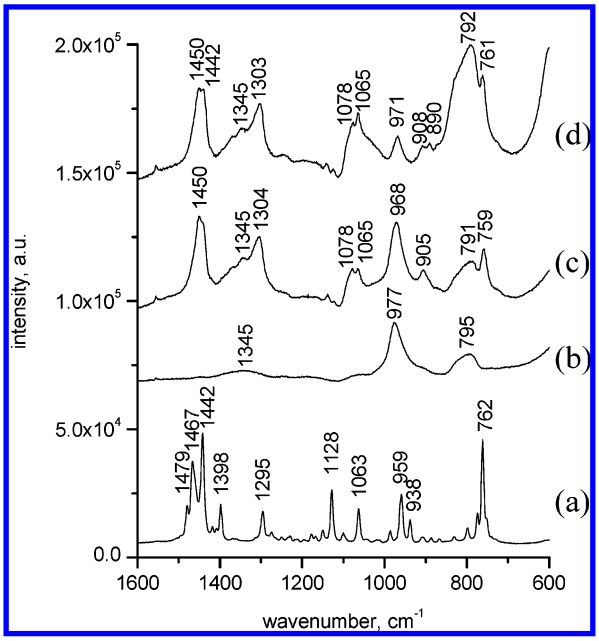

Figure 8. Raman spectra of (a) reagent crystalline CTAB, (b) wet silica nanoparticles, (c) wet silica nanoparticles with sorbed CTA^+ at approximately a monolayer surface coverage, and (d) wet silica nanoparticles with sorbed CTA^+ at approximately a bilayer surface coverage.

In the 1500−700 cm^{-1} region, the spectra of pure SiO_2 nanocolloids showed a strong band at 977 cm^{-1} and a relatively weak band at 795 cm^{-1}, both of which are attributed to stretching vibrations of surface Si−O bonds (Figure 8b). These bands shifted to low wavenumbers by 3−9 cm^{-1} with sorbed CTA^+, again suggesting the interactions between Si−O functional groups and the CTAB headgroups. For pure crystalline CTAB solids (Figure 8a), the following spectral bands were observed: the CH_2 bending modes (1430−1480 cm^{-1}), the CH_2 twisting mode (∼1300 cm^{-1}), the skeletal vibration modes (1130−1050 cm^{-1}), and the CH_3 rocking mode (∼760 cm^{-1}). The CH_2 bending mode gives splitting at 1467 and 1442 cm^{-1} because of strong hydrocarbon chain interactions in a highly ordered arrangement. However, for sorbed CTA^+ on SiO_2 surfaces (Figure 8c and d), the splitting disappeared, again indicating a flexible hydrocarbon chain arrangement as discussed earlier. Bands at ∼1064 and 1078 cm^{-1} can be assigned to the C−C stretching vibration mode in all-trans configurations and gauche conformations, respectively. The C−C stretching vibration modes are affected by the intrachain disorder, and the height ratio, I_{1064}/I_{1078}, has been used to measure the trans−gauche isomerization.[43,44] For pure solid CTAB, only a single band at ∼1063 cm^{-1} was observed, indicating an all-trans conformation of CTAB molecules (Figure 8a). While in the adsorbed states (Figure 8c and d), two Raman bands at ∼1078 and 1065 cm^{-1} could be clearly discerned, indicating the gauche conformation of sorbed CTA^+ molecules on the surface. These observations again demonstrate that CTA^+ hydrocarbon chains are mobile in sorbed layers on silica surfaces, and the results are consistent with the FTIR measurements. Both the FTIR and Raman spectroscopic data thus support the adsorption mechanism of the reverse orientation model for CTA^+ sorption on porous SiO_2 nanoparticles.[16,25]

Conclusion

In conclusion, our studies show that CTA^+ cations and SiO_2 colloidal nanoparticles have strong interaction. The adsorbed CTA^+ cations significantly affect the SiO_2 colloidal surface property and stability. The ζ potential (or surface charge) increased consistently with an increase in CTA^+ sorption on SiO_2 at low CTAB concentration, which caused a destabilization of the colloid suspension. A complete flocculation of SiO_2 colloids occurred at about zero ζ potential (near to ZPC). The electrostatic interaction effect is dominant in the flocculation process. However, with further increase in CTA^+ sorption, a charge reversal was observed and caused a restabilization of the SiO_2 colloids. At its maximum sorption capacity, the measured zeta potential (+40 mV) corresponded closely to the negative potential of uncoated SiO_2 nanoparticles (−50 mV). Adsorption amount measurement suggests that a bilayer of CTA^+ forms on SiO_2 surfaces at the saturate adsorption. The FTIR and Raman spectroscopic analysis confirmed that the CTA^+ cations are bound to the SiO_2 surface via their headgroup which formed the first layer of the bilayer, while the second layer was adsorbed via hydrophobic interaction between hydrocarbon tails of CTA^+ cations. In this study, the adsorption mechanism of CTA^+ on porous SiO_2 nanoparticles is in agreement with reverse orientation model.

Acknowledgment. This research was supported by the Office of Basic Energy Sciences, U.S. Department of Energy, under contract DE-AC05-00OR22725, with Oak Ridge National Laboratory, which is managed by UT-Battelle, LLC.

References and Notes

(1) Esumi, K, J. *Colloid Interface Sci.* **2001**, *241*, 1.
(2) Clunie, J. S.; Ingram, B. T. In *Adsorption from Solution at the Solid/Liquid Interface*; Parfitt, G. D., Rochester, C. H., Eds.; Academic Press: New York, 1983; p 105.
(3) Esumi, K.; Nagahama, T.; Meguro, K. *Colloids Surf.* **1991**, *57*, 149.
(4) Monticone, V.; Treiner, C. J. *Colloid Interface Sci.* **1994**, *166*, 394.
(5) Goloub, T. P.; Koopal, L. K.; Bijsterbosch, B. H. *Langmuir* **1996**, *12*, 3188.
(6) Kitiyanan, B.; O'Haver, J. H.; Harwell, J. H.; Osuwan, S. *Langmuir* **1996**, *12*, 2162.
(7) Esumi, K.; Mizutani, H.; Shoji, K.; Miyazaki, M.; Torigoe, K.; Yoshimura, T.; Koide, Y.; Shosenji, H. J. *Colloid Interface Sci.* **1999**, *220*, 170.
(8) Szekeres, M.; Dékány, I.; de Keizer, A. *Colloids Surf.* **1998**, *141*, 327.
(9) Atkin, R.; Craig, V. S. J.; Biggs, S. *Langmuir* **2000**, *16*, 9374.
(10) Churaev, N. V.; Sergeeva, I. P.; Sobolev, V. D.; Jacobasch, H, -J.; Weidenhammer, P.; Schmitt, F.-J. *Colloids Surf.* **2000**, *164*, 121.
(11) Kung, K.-H. S.; Hayes, K. F. *Langmuir* **1993**, *9*, 263.
(12) Neivandt, D. J.; Gee, M. L.; Hair, M. L.; Tripp, C. P. *J. Phys. Chem. B* **1998**, *102*, 5107.
(13) Chernyshova, I. V.; Rao, K. H.; Vidyadhar, A.; Shchukarev, A. V. *Langmuir* **2000**, *16*, 8071.
(14) Esumi, K.; Matoba, M.; Yamanaka, Y. *Langmuir* **1996**, *12*, 2130.
(15) Esumi, K.; Goino, M.; Koide, Y. J. *Colloid Interface Sci.* **1996**, *183*, 539.
(16) Fan, A.; Somasundaran, P.; Turro, N. J. *Langmuir* **1997**, *13*, 506.
(17) Levitz, P.; van Danme, H.; Keravis, D. *J. Phys. Chem.* **1984**, *88*, 2228.
(18) Atkin, R.; Craig, S. J.; Biggs, S. *Langmuir* **2001**, *17*, 6155.
(19) Liu, J. F.; Min, G.; Ducker, W. A. *Langmuir* **2001**, *17*, 4895.
(20) Fleming, B. D.; Biggs, S.; Wanless, E. J. *J. Phys. Chem. B* **2001**, *105*, 9537.
(21) Rennie, A. R.; Lee, E. M.; Simister, E. A.; Thomas, R. K. *Langmuir* **1990**, *6*, 1031.
(22) Cummins, P. G.; Staples, E.; Penfold, J. *J. Phys. Chem.* **1990**, *94*, 3740.
(23) Schulz, J. C.; Warr, G. G.; Butler, P. D.; Hamilton, W. A. *Phys. Rev. E* **2001**, *63*, 041604.
(24) Green, R. J.; Su, T. J.; Lu, J. R.; Webster, J. R. P. *J. Phys. Chem. B* **2001**, *105*, 9331.
(25) Somasundaran, P.; Fuerstenau, D. W. *J. Phys. Chem.* **1966**, *70*, 90.
(26) Harwell, J. H.; Hoskins, J. C.; Schechter, R. S.; Wade, W. H. *Langmuir* **1985**, *1*, 251.
(27) Gu, T.; Huang, Z. *Colloids Surf.* **1989**, *40*, 71.

(28) Gu, T.; Rupprecht, H.; Galera-Gómez, P. A. *Colloid Polym. Sci.* **1993**, *271*, 799.
(29) Stöber, W.; Fink, A.; Bohn, E. *J. Colloid Interface Sci.* **1968**, *26*, 62.
(30) Eskilsson, K.; Yaminsky, V. V. *Langmuir* **1998**, *14*, 2444.
(31) Furst, E. M.; Pagac, E. S.; Tilton, R. D. *Ind. Eng. Chem. Res.* **1996**, *35*, 1566.
(32) Horváth-Szabó, G.; Høiland, H. J. *Colloid Interface Sci.* **1996**, *177*, 568.
(33) de Keizer, A.; van der Ent, E. M.; Koopal, L. K. *Colloids Surf.* **1998**, *142*, 303.
(34) Kosmulski, M. J. *Colloid Interface Sci.* **2002**, *253*, 77.
(35) Vansant, E. F.; Van Der Voort, P.; Vrancken, K. C. *Characterization and Chemical Modification of the Silica Surface*; Elsevier: Amsterdam, 1995.
(36) Coretsky, C. M.; Sverjensky, D. A.; Salisbury, J. W.; D'Aria, D. M. *Geochim. Cosmochim. Acta* **1997**, *61*, 2193.
(37) Wang, W.; Li, L.; Xi, S. *J. Colloid Interface Sci*. **1993**, *155*, 369.
(38) Wang, W.; Li, L.; Xi, S. *Chin. J. Chem. Phys.* **1993**, *6*, 553.
(39) Casal, H. L.; Cameron, D. G.; Smith, I. C. P.; Mantsch, H. H. *Biochemistry* **1980**, *19*, 444.
(40) Cameron, D. G.; Casal, H. L.; Mantsch, H. H. *Biochemistry* **1980**, *19*, 3665.
(41) Synder, R. G. *J. Mol. Spectrosc*. **1961**, *7*, 116.
(42) Umemura, J.; Cameron, D. J.; Mantsch, H. H. *Biochim. Biophys. Acta* **1980**, *602*, 32.
(43) Snyder, R. G.; Scherer, J. R.; Gaber, B. P. *Biochim. Biophys. Acta* **1980**, *601*, 47.
(44) Gaber, B. P.; Petitcolas, W. L. *Biochim. Biophys. Acta* **1977**, *465*, 260.